remote sensing

MDPI

Article

Using a Multiobjective Genetic Algorithm to Design Satellite Constellations for Recovering Earth System Mass Change

Carlos M. A. Deccia [1,*], David N. Wiese [2] and Robert S. Nerem [1]

[1] Colorado Center for Astrodynamics Research, Ann and H.J. Smead Department of Aerospace Engineering Sciences, University of Colorado Boulder, Boulder, CO 80303, USA; nerem@colorado.edu
[2] Jet Propulsion Laboratory, California Institute of Technology, Pasadena, CA 91109, USA; david.n.wiese@jpl.nasa.gov
* Correspondence: carlos.deccia@colorado.edu

Abstract: The Gravity Recovery and Climate Experiment (GRACE) and GRACE Follow-On (GRACE-FO) provided twenty years of data on Earth's time-varying gravity field. Due to their design, GRACE and GRACE-FO are inherently limited in their spatiotemporal coverage, limiting their resolution to a few hundred kilometers and temporally to roughly monthly solutions. To increase the global spatiotemporal resolution and allow for the determination of submonthly time-varying gravity field signals, a constellation of GRACE-type satellite pairs is a possible path forward. Advances in small form factor instrumentation for small satellites have become progressively inexpensive, reliable, and of higher quality. This leads us to consider that a constellation of GRACE-type small satellites could be part of future gravimetric satellite missions. In this work, we investigate the viability and limitations of a genetic-algorithm-based optimization and its objective function to generate satellite constellations to recover daily Earth system mass changes. The developed approach is used to create satellite constellations that are optimally designed to recover gravity variations of sufficient resolution at a range of temporal frequencies (i.e., daily to monthly). We analyze a constellation's performance using a combination of observability in space, accounting for directionality, and homogeneity in time. This allows us to navigate through a vast search space in a relatively short period of time and estimate the relative performance of constellations to each other. Using evolutionary theory, we converge towards a set of optimally selected orbits. The characteristics of the designed constellations have been validated using high-fidelity numerical simulations. We summarize these results and discuss their implications for possible future constellations of small GRACE-like satellite pairs. The resulting constellations have an inherently improved spatiotemporal performance, which reduces temporal aliasing errors and allows the characterization of daily mass-change effects.

Keywords: constellation design; genetic algorithm; optimization; temporal aliasing; mass change observations; gravity recovery and climate experiment; GRACE; GRACE-follow on

check for updates

Citation: Deccia, C.M.A.; Wiese, D.N.; Nerem, R.S. Using a Multiobjective Genetic Algorithm to Design Satellite Constellations for Recovering Earth System Mass Change. *Remote Sens.* **2022**, *14*, 3340. https://doi.org/10.3390/rs14143340

Academic Editor: Jianguo Yan

Received: 21 April 2022
Accepted: 1 July 2022
Published: 11 July 2022

Publisher's Note: MDPI stays neutral with regard to jurisdictional claims in published maps and institutional affiliations.

Copyright: © 2022 by the authors. Licensee MDPI, Basel, Switzerland. This article is an open access article distributed under the terms and conditions of the Creative Commons Attribution (CC BY) license (https://creativecommons.org/licenses/by/4.0/).

1. Introduction

Since 2002, the Gravity Recovery and Climate Experiment (GRACE) satellite mission has provided the scientific community with invaluable gravimetric data [1,2]. By measuring Earth's monthly time-variable gravity field from 2002 to 2017, it allowed us to infer natural fluctuations and anthropogenic fingerprints on the Earth's global water cycle. This includes areas such as determining changes in continental hydrology and ocean bottom pressure [3,4]. It allowed us to characterize the global melting of glaciers and ice sheets through the measurement of their mass loss (∼600 Gt/year) [5]—the rate at which ocean mass is contributing to sea-level rise [6]. The societal and scientific value of mass transport data obtained from GRACE has been recognized in such a manner that a successor to GRACE-FO was recommended as one of five designated missions within the decade following GRACE (2017–2027) in the National Academy of Sciences Decadal Survey for

Earth Science and Applications from Space [7]. The successive mission, GRACE Follow-On (GRACE-FO) [8], has continued the monthly mapping of Earth's time-variable gravity field since 2018. Due to GRACE and GRACE-FO's single polar pair mission architecture, full global coverage for a single pair can take up to 30 days for spatial resolutions of a few hundred kilometers, thus leading to a spatial and temporal resolution of the detected signals of $\sim$300 km^2 and 30 days, respectively. This means that signals at higher spatial and temporal resolutions, such as rapid flooding events, cannot be quantified [9]. These mission architectures are limited in their spatiotemporal performance. They are affected by temporal aliasing errors, which are caused due to undersampling of submonthly geophysical signals, corrupting the gravity solution. A higher frequency sampling of the gravity field would be a straightforward method to reduce such errors. Recently, there has been a request by the community for data products with increased spatiotemporal resolution [10]. Past mission analyses have tackled this problem by comparing the improvement of a two-pair GRACE-like (i.e., low–low satellite–satellite tracking) constellation to a single-pair configuration [11–14].

An n_{pair} GRACE-like satellite constellation is a possible solution to reach higher spatiotemporal resolutions and resolve submonthly gravity field signals. Due to technological advances in small satellite technology, many scientific missions can be fulfilled with small satellite hardware [15–19]. Several groups [20,21] have been exploring the possibility of collecting GRACE-type intersatellite ranging measurements from smallsats or cubesats, which would dramatically decrease the costs of the satellites. This is a critical path to pursue, as the implementation of new gravity-sensing technologies (atom interferometry, etc.) are still some years away [22]. A constellation composed of small satellites could allow for higher spatial and temporal resolution as well as multiple decades of observations since it lacks single-point failures that are present in single pair satellite constellations. Should one satellite or satellite pair stop functioning, it would not disrupt the rest of the constellation to carry on the mission, albeit potentially with limited capability [23–28]. The relatively large number of satellites in the constellation would additionally drive the cost down by enabling the production of instrumentation in larger numbers [29,30]. Creating the appropriate tools and verifying them by performing corresponding simulations in a high-fidelity environment is necessary to optimize such an n_{pair} GRACE-like mission design. This paper aims to design a methodology that, given a set of constraints, optimizes the orbital configuration of a GRACE-like constellation for the recovery of temporal gravity field variations.

2. Methodology

The main issue with generating an n_{pair} satellite constellation is the size of the search space. When considering constellations with one or two satellite pairs, it is possible to perform a Monte Carlo study [31]; however, with an increasing number of pairs, the size of the search space grows exponentially. To explore the search field efficiently, we use a genetic algorithm (GA). These stochastic search methods take their inspiration from Darwin's theory of natural evolution [32]. In this study, the GA analyzes a set of constellations that define the population at each generation. Each constellation contains a set of GRACE-like n_{pair} satellites. The relevant characteristics of each constellation are encoded as a string of bits that can be either zeros or ones. We analyzed the impact of three orbital parameters for this investigation: the inclination i, right ascension of the ascending node Ω, and mean anomaly M. These orbital elements are encoded to span the whole viable search space of constellation configurations' characteristics. The altitude is fixed at 500 ± 5 km. The designed constellations fly in circular orbits to avoid changes in relative distance due to eccentric orbits. In this paper, the authors selected a constellation consisting of six GRACE-like pairs to verify the described methodology. Previous design points suggest it to be the smallest constellation size to recover reasonable time-varying gravity fields at daily time intervals [33].

The resulting populations are then evaluated by measuring their so-called fitness value, determined by an objective function, described in Section 2.1. This function is defined by the characteristic we intend to optimize (e.g., spatial and temporal resolution). Once these fitness values are obtained, they serve as a quality metric in the GA for each population. GA operators utilize them to improve the set of solutions for the next generation. The genetic algorithm is a formidable search algorithm that is capable of dealing with a very large discrete search space [34]. GAs use biological and computationally principled methods to explore a given number of variables. Using techniques to balance exploration against exploitation, the search space is efficiently explored for candidate n_{pair} satellite constellations. There is no proof of convergence, but with a large population and multiple runs, the probability of finding a global optimum can be maximized. A potent type of GA is the Multiobjective Genetic Algorithms (MOGA) that allow for more than one objective function to be optimized simultaneously. The main drawback of this method is that the complexity directly correlates to the number of objectives and the size of the selected population.

To circumvent this issue, we make use of the Nondominated Sorting Genetic Algorithm II (NSGA-II) developed by Deb [35]. A flowchart depicting the NSGA-II algorithm can be seen in Figure 1. This method uses a fast nondominated sorting approach and encourages diversity of solutions, with a quick convergence, and has an aptness for global optimization. Additionally, it decreases computational complexity.

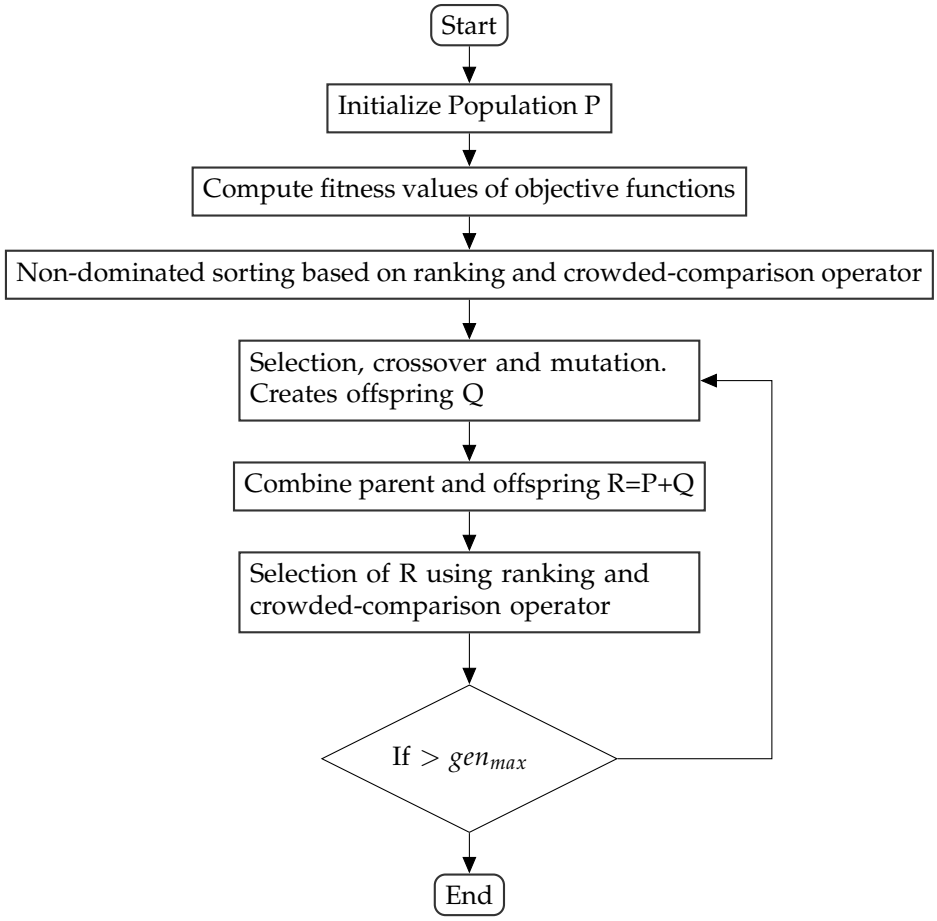

Figure 1. Algorithm scheme of the nondominated sorting genetic algorithm II (NSGA-II).

Starting from a set of constellations, called populations, picked at random, it computes the fitness of each constellation by an objective function, described in Section 2.1, which we have developed specifically for a GRACE-like multipair constellation. Figure 2 shows a sample figure of individual constellations, represented by dots, on a search space spanned

by two objective functions: J_{so} on the x-axis and J_{to} on the y-axis. These constellations are organized by the their fitness values onto Pareto curves, which act as a ranking metric. The Pareto curve closest to the axes origin, also called the optimality point, is ranked higher than each subsequent front. Each of these Pareto curves can have one or more constellations assigned to it and are equivalent to what the GA considers their quality to be. The closer these Pareto curves are to the optimality point, the more desirable they are. The GA then takes the solutions within the best Pareto curves; they are defined as the "parents" and use them to create new solutions. Each constellation is encoded as a binary string. By recombination of the strings of selected "parents", new constellations, called "children", are created and will define the next generation with the previous best Pareto curves. Furthermore, a random mutation is introduced by randomly changing a single bit. A crowded-comparison operator is applied in order to incentivize diversity in the selected solutions leading the algorithm toward a uniformly spread-out Pareto-optimal front. This procedure is repeated at each generation until convergence has been hit or a select number of generations has been reached. The NSGA-II scheme is well-established and has been used in various constellation designs [36–41].

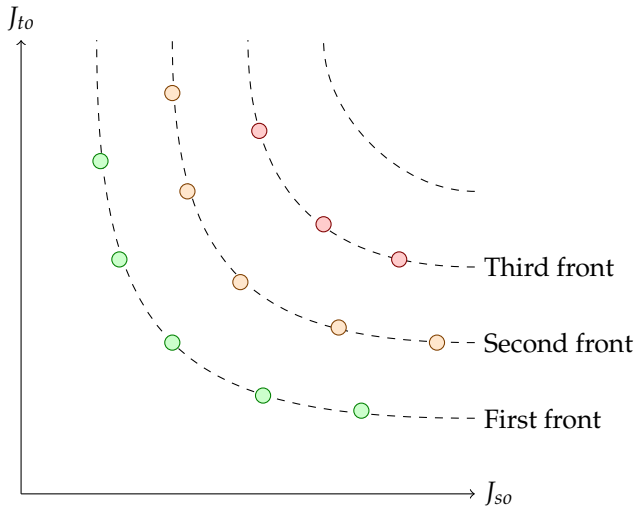

Figure 2. Pareto front characterization relative to the search space defined by the objective functions J_{so} and J_{tv}.

2.1. Objective Function

To analyze the fitness of each constellation, we make use of the objective functions J_{so} and J_{to}. J_{so} represents the objective value analyzing the global spatial fitness, whereas J_{to} is the analog value for the global temporal fitness. Both objective values are being optimized simultaneously through the multiobjective NSGA-II algorithm.

2.1.1. Spatial Objective Function J_{so}

For the analysis of the spatial domain, we make use of a 3° equal-area spatial grid cell since it corresponds to the ∼300 km^2 native spatial resolution of current mass change estimates [42]. This subdivision divides the surface of Earth into 4551 equal-area cells, as shown in Figure 3, which will be represented herein by m. If the spacecrafts' ground track, which is sampled at a 5 s interval, is over a specific spatial grid cell, this one is considered to be observed in its entirety once.

For the purposes of describing the spatial fitness, the spatial objective function in Equation (1) is composed of four distinct subobjectives—J_{ob}, J_{ro}, J_{ew}, and J_{ns}—which are calibrated using their own individual weighting factors W_{ob}, W_{ro}, W_{ew}, and W_{ns}, respectively. More to the selection of these values in Section 2.1.2.

$$J_{so} = W_{ob} \cdot J_{ob} + W_{ro} \cdot J_{ro} + W_{ew} \cdot J_{ew} + W_{ns} \cdot J_{ns} \quad (1)$$

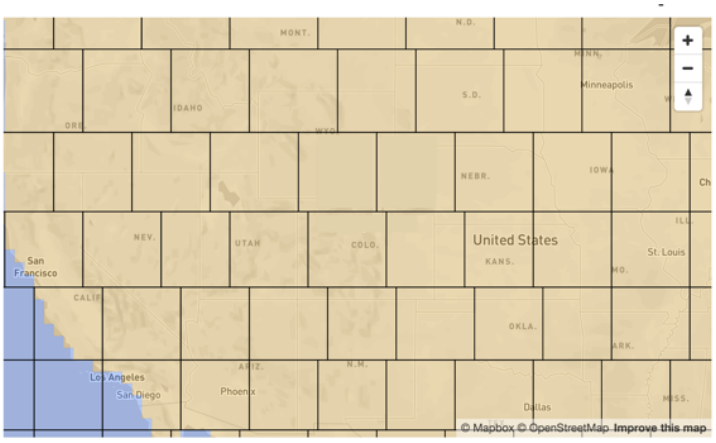

Figure 3. Three degrees equal-area spatial grid cells [43].

The first spatial subobjective function, J_{ob}, describes how the global coverage function J_{so} is related to the overall observability of the system. Here, we compare the sum of observed spatial grid cells N to the total number of cells available m, where i stands for the subscript that identifies each spatial cell. A cell is observed if at least one satellite pair that makes up a constellation measures the corresponding spatial cell. This relation can be seen in Equation (2).

$$J_{ob} = 1 - \frac{\sum_{i=1}^{m} N_i}{m} \tag{2}$$

For the second parameter of Equation (1), we focus on the uniformity of repeat observations. Here, we make use of the Gini coefficient. Corrado Gini originally developed this method in 1912 to describe income inequality for economic systems [44]. The application of this coefficient using repeat observations is shown in Equation (3). Here, M stands for the number of times a spatial grid cell has been observed more than once and i and j stand for the subscript that identifies the corresponding spatial cell. The resulting Gini coefficient in Equation (3) has a value that ranges between zero and one and represents how uniformly all spatial cells have been observed more than once, where zero stands for a perfectly uniform system in terms of repeated observations.

$$J_{ro} = \frac{\sum_{i=1}^{m} \sum_{j=1}^{m} |M_i - M_j|}{2m \sum_{i=1}^{m} M_i} \tag{3}$$

A visual representation of the behavior of the Gini coefficient adapted for this constellation design can be seen in Figure 4. The Gini coefficient drives the objective function to create constellations in which the number of revisits of each spatial grid cell is as uniformly distributed as possible. This directs the optimization function to seek globally uniform solutions concerning how often the constellation has revisited each spatial cell. A zero value equals an ideal constellation where a percentage of the spatial cells have observed the same percentage of observations. The opposite would be the case for a Gini coefficient of one, where a small percentage of spatial cells have observed a high percentage of observations.

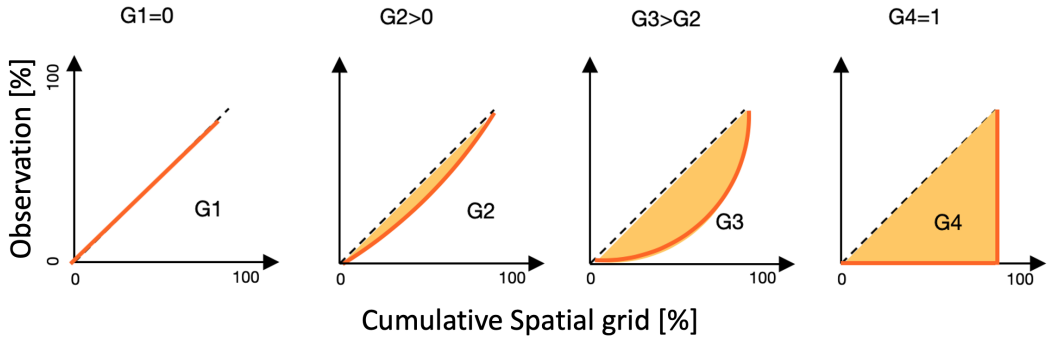

Figure 4. The behavior of the Gini coefficient, as described in [44], adapted for a spatial grid cell analysis. A uniform distribution is defined when an equal percentage of the spatial grid observes the same percentage of the observations throughout the spatial domain (G1). The least desirable case (G4) occurs when a small percentage of the spatial grid observes a high percentage of the total observations. Cases G2 and G3 are intermediary stages.

At least one GRACE-like pair within a constellation must be in a polar orbit to ensure global coverage. As we know from GRACE simulations, this gives us a good estimation of North–South information but lacks East–West information, leading to correlated errors in GRACE data manifesting as striping in unfiltered GRACE-derived gravity maps [45].

The last two subobjective functions of Equation (1) analyze the directionality of the ground track at each spatial grid cell, shown in Figure 5, as a description for the quality of East–West and North–South information that is present in each satellite constellation.

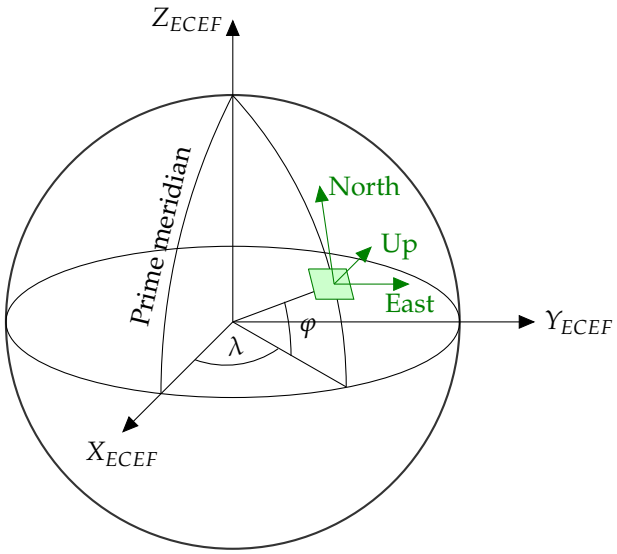

Figure 5. Relation of the local reference frame to the Earth-centered, Earth-fixed (ECEF) coordinate system used to describe the quality of the North–South and East–West information produced by the constellation ground track. The ECEF coordinates are shown in relation to the longitude (λ) and latitude (φ).

First, we transform the velocities of all observations at each spatial grid cell to a local frame with Equation (4), where the vectors $\hat{\mathbf{R}}\hat{\mathbf{E}}\hat{\mathbf{N}}$ represent the radial, east, and north direction. Subsequently, we superposition the local velocities for all spatial cells to form matrix $\mathbf{A}$ by disregarding the radial velocity component since it does not add any

information to the velocity vector's East–West and North–South local components. The size of matrix **A** is $2 \times n$, where n identifies the number of observations at each spatial cell.

$$\vec{\mathbf{v}}_{local} = \left[\hat{\mathbf{R}}\hat{\mathbf{E}}\hat{\mathbf{N}}\right]\vec{\mathbf{v}}_{ECEF} \qquad \mathbf{A} = \begin{bmatrix} \hat{\mathbf{v}}_1 \\ \vdots \\ \hat{\mathbf{v}}_n \end{bmatrix} \tag{4}$$

The diagonal elements of the **B** matrix define how much information the system has in the East–West compared with the North–South direction at each spatial cell.

$$1 - \frac{\mathbf{A}^T\mathbf{A}}{n} = \begin{bmatrix} B_{ew} & B_{cross} \\ B_{cross} & B_{ns} \end{bmatrix} \tag{5}$$

A visual representation of how the B_{ew} value varies depending on which satellite constellation is analyzed can be seen in Figure 6.

Here, a two-pair satellite constellation has been used to illustrate the effect of the East–West information on the objective function. The first pair has been chosen to be polar, whereas the second pair has a varying inclination between 50° and 80°. The two-pair solution with the second pair at 50° has very good East–West information in the equatorial region; still, it is missing all the information in the polar region. The case with the second pair at 80° is the direct opposite, where it has excellent East–West information coverage over the high latitudes but is missing the equatorial region. An ideal middle ground is the solutions at 60° and 70°, which cover just enough of the equatorial region as well as part of the high-latitude regions. From previous research, we know that a possible mathematical optimum when analyzing the East–West information is at 63° of inclination [46]. As we can see through visual inspection of Figure 6, the increase in inclination of the second pair is correlated to a better overall value for the B_{ew} information up to an inclination between 60° and 70°. By adding additional pairs at various inclinations, there is a superposition of the collected cross-track information of all pairs that make up a constellation into a single combined solution.

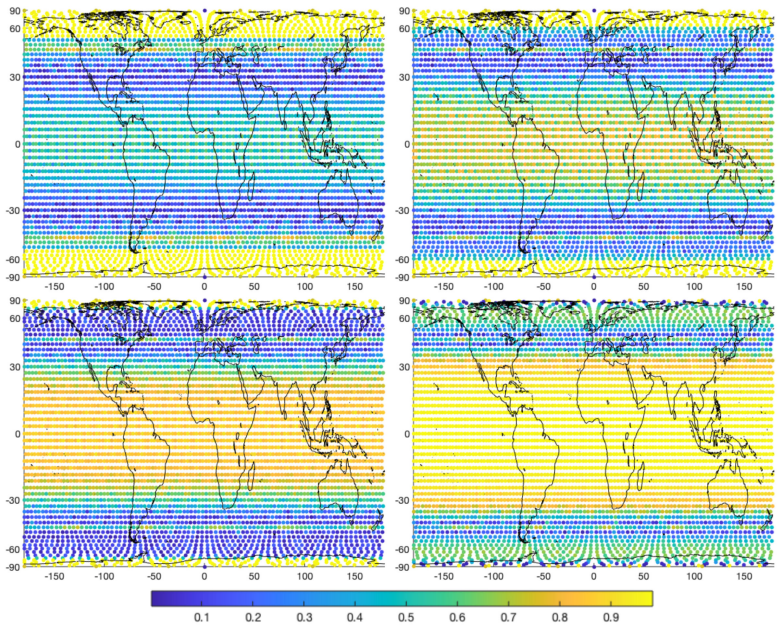

Figure 6. B_{ew} information for a two-satellite-pair example with a polar pair and an inclined pair of 50° (**top left**), 60° (**top right**), 70° (**bottom left**), and 80° (**bottom right**). A lower value of B_{ew} directly relates to beneficial information in the East-West direction due to the ground track directionality. The global value is optimum between the inclinations of 60° and 70°.

An appropriate metric for the quality of the information present in both the East-West B_{ew} and North-South B_{ns} information for all spatial cells m is one where both the average as well as the uniformity of such information are optimized. This relation is shown in Equations (6) and (7).

$$\mathbf{B}_{ew} = \begin{bmatrix} B_{ew_1} \\ \vdots \\ B_{ew_m} \end{bmatrix}, \mathbf{B}_{ns} = \begin{bmatrix} B_{ns_1} \\ \vdots \\ B_{ns_m} \end{bmatrix} \tag{6}$$

$$\begin{aligned} J_{ew} &= \frac{\overline{\mathbf{B}_{ew}}}{2} + \frac{1}{2}\left(\frac{\sum_{i=1}^{m}\sum_{j=1}^{m}|B_{ew_i} - B_{ew_j}|}{2m\sum_{i=1}^{m}B_{ew_i}}\right) \\ J_{ns} &= \frac{\overline{\mathbf{B}_{ns}}}{2} + \frac{1}{2}\left(\frac{\sum_{i=1}^{m}\sum_{j=1}^{m}|B_{ns_i} - B_{ns_j}|}{2m\sum_{i=1}^{m}B_{ns_i}}\right) \end{aligned} \tag{7}$$

2.1.2. Weight Calibration

Having characterized the spatial objective values, the next step is to identify appropriate values for their corresponding weights. All objective values have been described to give values between zero and one, where the lower the value, the closer the objective value is to the mathematically ideal configuration.

These four objective functions could be equally weighted; however, we know observability is of paramount importance. Therefore, W_{ob} has been overweighted with a value of 100, which leads one of the satellite pairs in the resulting constellation to be a polar or near-polar pair. The subsequent three weights W_{ro}, W_{ew}, and W_{ns} represent the weights regarding repeat observations and the ground track directionality per spatial grid cell. We started with an equal value of 1 for these weights, which is a valid selection for celestial objects such as the moon or Mars, or when one would like to consider a static gravity field solely. Through a literature search on the importance of geophysical variables [7], as well as previous design points [11], we calibrated these weights based on this prior information to capture equally hydrology, ocean, and ice mass variations. The North–South ground track directionality helps obtain information about these areas of interest to a higher degree than the East–West ground track directionality and repeat observations, which is why it is more heavily weighted. The main drive for this is the recovery of ice mass variations present at high-latitude areas driving the solution away from mathematically optimal solutions should all areas of interest be uniformly distributed on Earth. The resulting weight values can be found in Table 1.

Table 1. Spatial objective weights.

Weight	Value [−]
W_{ob}	100
W_{ro}	1
W_{ew}	1
W_{ns}	10

2.1.3. Temporal Objective Function J_{to}

For each spatial grid cell, we analyze the temporal coverage by using a grid in the time dimension. These temporal grid cells are characterized by their time size and corresponding spatial grid cell.

Figure 7 shows an example of a representation of the temporal grid cells at each spatial cell for the period of one day. Here, a signal in black is shown where star signs

represent the samples taken by the spacecraft. The signal runs between time t_0 and t_{day} and is subdivided into 16 temporal cells. Analog to the spatial cells, as long as one sample is within the limits of a temporal cell, this cell is considered to be observed in its entirety. Sixteen temporal grid cells for each day of observation are chosen to balance having a sufficiently fine temporal grid cell size that meets the sampling criteria of one temporal cell per orbital revolution with the available computational limitations. The signals of interest chosen for the verification of this methodology, described in Section 4, have a 3-hour temporal resolution. This requires us to seek a temporal resolution of at least 1.5 h, leading to 16 temporal grid cells per day.

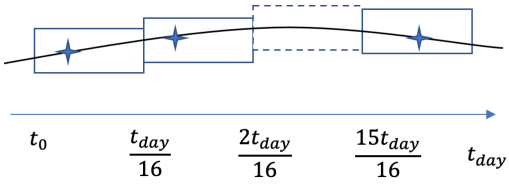

Figure 7. Temporal grid cells at a given spatial cell for the period of one day.

Each temporal cell TC in Equation (8) represents a binary representation if a specific cell has been observed, where T stands for the number of days analyzed. Through a reformulation in vector form, we can apply the Gini coefficient in Equation (9), which represents the uniformity of each spatial cell in time ($\mathbf{G}_{TV}$). Equation (10) uses the previously computed Gini $\mathbf{G}_{TV}$ to optimize the average as well as the uniformity of all spatial grid cells to each other.

$$\begin{bmatrix} TC_{1,1} & \dots & TC_{1,16\cdot T} \\ \vdots & \ddots & \vdots \\ TC_{m,1} & \dots & TC_{m,16\cdot T} \end{bmatrix} = \begin{bmatrix} \mathbf{TV}_1 \\ \vdots \\ \mathbf{TV}_m \end{bmatrix} \tag{8}$$

$$\mathbf{G}_{TV} = \frac{\sum_{i=1}^{m}\sum_{j=1}^{m}|\mathbf{TV}_i - \mathbf{TV}_j|}{2m\sum_{i=1}^{m}\mathbf{TV}_i} \tag{9}$$

$$J_{to} = \frac{\overline{\mathbf{G}_{TV}}}{2} + \frac{1}{2}\left(\frac{\sum_{i=1}^{m}\sum_{j=1}^{m}|\mathbf{G}_{TV_i} - \mathbf{G}_{TV_j}|}{2m\sum_{i=1}^{m}\mathbf{G}_{TV_i}}\right) \tag{10}$$

This defines the temporal objective function J_{to} and will allow for a uniform solution both for the whole time of analysis (29 days) as well as over shorter periods. Due to the nondominated sorting approach used in NSGA-II, there is no need to apply weights to the spatial and temporal objective functions J_so and J_to. This concludes the description of the objective functions used in the genetic algorithm.

3. Orbital Considerations

Given the objective function described in Section 2, this section aims to characterize the selected parameters used in the configuration for the numerical search algorithm. These variables are summarized in Table 2.

Table 2. Fixed and variable parameters used in the optimization process.

Parameter	Value	Unit
Propagation time (T)	29	(day)
Satellite pairs (n_{pairs})	6	(pairs)
Orbit altitude (h_{alt})	500 ± 5	(km)
Repeat period (RP)	29	(day)
Eccentricity (e)	0	(-)
Arg. of perigee (ω)	90	(°)
Intersatellite distance (r_{int})	100	(km)
Spatial cell (SC)	4551	(-)
Temporal cell (TC)	16	(per-day)
Inclination (i)	[0–180]	(°)
RAAN (Ω)	[0–360]	(°)
Mean anomaly (M)	[0–360]	(°)

In the analysis of geophysical signals [7], monthly solutions are of high interest. For this reason, we chose to optimize the constellation design for a propagation time T of 29 days. Altitude is the most critical design variable for a satellite gravity mission. The closer the satellite constellation orbits around Earth, the higher the strength of geophysical signals detected. However, the choice of altitude drives the satellite design and targeted lifetime. At lower altitudes, the orbital period of the satellites is faster, allowing them to observe a higher percentage of Earth in a shorter time. At the same time, flying at low altitudes would require the addition of drag compensation to extend the mission lifetime to reach GRACE-like levels. If the GA had a free choice in altitude, it would tend to select constellations at low altitudes. Due to this, the user must choose an altitude range as a fixed parameter rather than allow it to be a free parameter. To guarantee consistency in the constellation coverage, all pairs' orbits have been constrained to repeat orbits of 29 days at an altitude of 500 ± 5 km. Realistically, the constellation should incorporate some orbit maintenance capability to maintain the orbits at their repeat period. To guarantee the same levels of geophysical signal strength experienced by each pair throughout their orbit, we chose an eccentricity equal to zero. Additional values that have been fixed are the argument of perigee and the intersatellite distance at 90° and 100 km, respectively. To verify the viability of this tool, we chose six GRACE-like pairs for the forthcoming simulations. As previously discussed in Section 2, the spatial and temporal grid have been selected to be 16 and 4551, respectively. These values correspond to a temporal sampling requirement of 1.5 h and a spatial 3° equal area. The parameters that we vary are inclination (i), right ascension of the ascending node (RAAN), and the mean anomaly (M). These can vary freely between prograde and retrograde values and, in the case of RAAN and M, across 360°.

4. Simulation Setup

To build a constellation of GRACE-type satellites, we make use of the two main simulation tools developed by NASA's Goddard Space Flight Center (GSFC)—GEODYN [47] and SOLVE [48]. GEODYN is GSFC's state-of-the-art geodetic parameter estimation and precision orbit determination system that implements an iterative weighted least squares estimation algorithm to solve for spherical harmonic coefficients. Once several satellite pairs have been simulated with GEODYN, they can be combined using SOLVE, a large linear systems solver that combines data of various days and configurations into one gravity field solution. To create realistic simulations, the models described in Table 3 are used for all forthcoming simulations. These models, truncated at degree and order 60, have subdaily temporal resolutions. The ECMWF and GLDAS models are provided at a 3 h temporal resolution where NCEP, OMCT, MOG2D, and the ESA ice model are defined with a 6 h temporal resolution. They represent the dominant mass variations for Earth.

Table 3. Simulation and model definitions.

Models	Truth	Nominal	Source
Static gravity field	EIGEN-GL04C	EIGEN-GL04C	[49]
Ocean tide	FES2004	GOT00	[50,51]
Atmospheric	ECMWF	NCEP	[52,53]
Ocean	OMCT	MOG2D	[54,55]
Hydrological	GLDAS	-	[56]
Ice	ESA	-	[57]

For the static gravity field, both the truth and nominal case have been selected to be equal since the static gravity field does not have any high-frequency mass variations and does not contribute to the temporal aliasing error. Different ocean tides, and atmospheric and ocean models have been chosen for both the truth and nominal cases. The difference in the ocean tide models is proportional to the tide models' error magnitude. In contrast, the difference between the atmospheric and ocean model represents the errors due to the atmosphere and ocean models.

The instrumentation on-board is assumed to be a microwave-ranging instrument, as is the case with the GRACE mission. This analysis considers satellite error sources, such as intersatellite ranging measurement, accelerometer, and GPS position errors. The satellite-to-satellite ranging measurement noise is described by a K-band microwave ranging system characterized by a white noise spectral density of 1.8 $\mu m/\sqrt{Hz}$ [12]. The spectral density of accelerometer errors in the radial and transversal directions are $(1 + 0.005/f)^{1/2} \times 10^{-10}$ $m/s^2/Hz^{1/2}$, and for the normal axis, is $(1 + 0.1/f)^{1/2} \times 10^{-9}$ $m/s^2/Hz^{1/2}$ [12]. The position errors due to GPS measurements are characterized by white noise with a standard deviation of 1 cm added to each of the three positions' axis [58]. A drag-compensated system will be assumed. The assumptions on instrument performance are based on identified intersatellite ranging and accelerometer technologies for SmallSat technologies from the Mass Change Designated Observable Study Team [59].

These simulations aim to recover the continental hydrology and ice mass variations. The simulations are performed in a series of steps. Given the initial conditions of a satellite pair, these are propagated using the defined set of truth models. The resulting output is the truth satellite-to-satellite range-rate data and satellite position. The previously defined range-rate measurement noise and accelerometer noise are superpositioned to the truth range-rate data. Errors to each of the three positions' axis of the satellites is added. This is a representation of the data resulting from a real GRACE-like mission. In the next step, the satellite's initial conditions and empirical satellite accelerations are estimated. For this, the set of the nominal force models is used in conjunction with the noisy range-rate and position data defined in the previous step. Lastly, the observation residuals and partial derivatives are estimated. In this step, we make use of the set of the nominal force models as well as—defined in the previous step—the noisy range-rate data, the estimated satellite initial conditions, and the estimated empirical satellite accelerations. The range-rate residuals are used to estimate the correction to the spacecraft state along with the geophysical spherical harmonic coefficients. For this, the state is converted to baseline elements and 9 out of the 12 elements are constrained [60]. The resulting one-day estimated solutions are combined using SOLVE to include all relevant days and pairs into one solution for the entire satellite constellation.

5. Results and Discussion

Given the objective function and the orbital considerations defined in Sections 2 and 3, we are seeking to verify a direct relationship between the numerical methodology characterized and the simulation setup in Section 4 that has been used in the literature to simulate GRACE-like constellations [7,11,23–28]. This will prove that the GA with its objective function can be used to numerically explore the search space for a wide variety of constellation configurations. This tool aims not to find a single solution but to narrow down the search

space and, at the same time, provide the mission designer with a family of constellation solutions that can fulfill the given requirements. This offers the constellation designer a variety of solutions that can be narrowed down based on other criteria (e.g., launch sites).

Figure 8 shows how the GA uses the objective function effectively to explore the search space, given here by the spatial and temporal objective function J. Within 20 generations, it has narrowed down the search space and identified a set of optimal solutions.

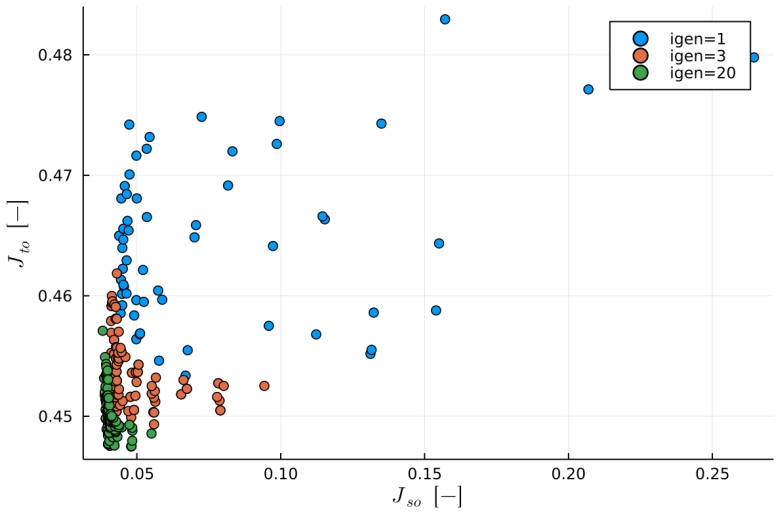

Figure 8. Constellation population for generations 1, 3, and 20. Each dot represents a different six-pair constellation. The values for the objective functions J_{so} and J_{to} are unitless.

The constellations generated at every generation are sorted on several Pareto curves using the fitness values evaluated by the objective functions. The closer the Pareto curves are to the optimality point, the higher the inherent quality of the constellations is in regard to the fitness values. To show how the information contained in the search space is in direct relation to the solutions of the simulations in Section 4, we analyze the constellations in the first generation and how its Pareto curves relate to simulation results given by the NASA/GSFC tools. The constellations developed in the first generation have been chosen due to having more significant variability in the computed fitness values resulting in a more extensive span in the quality of the analyzed constellations. Of all available Pareto curves in the first generation, Figure 9 shows four selected Pareto curves that encompass the entirety of the population in the first generation, namely, Pareto curves 1, 10, 48, and 98.

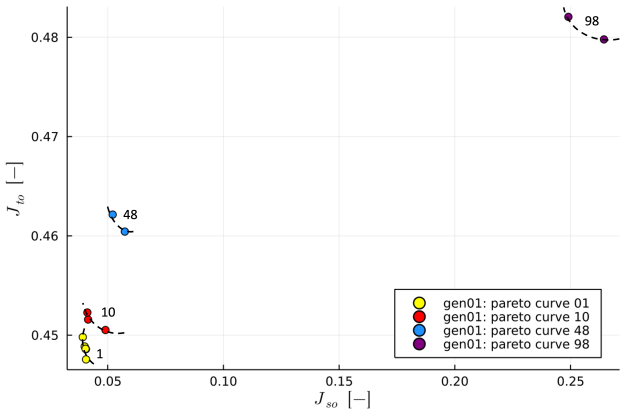

Figure 9. Pareto curves 1, 10, 48, and 98 span the search space both in spatial and temporal objective functions. The values for the objective functions J_{so} and J_{so} are unitless.

Using the simulation setup described in Section 4, we can verify with the degree variance curves in Figure 10 that there is a direct relationship between the location of the Pareto curves in the search space and the average quality of their solution represented in the degree variance format. Geoid degree error plots are constructed using the following equation:

$$\Delta N_n = r_{\oplus} \sqrt{\sum_{m=0}^{n} (\Delta \overline{C}_{nm}^2 + \Delta \overline{S}_{nm}^2)} \tag{11}$$

where

$$\begin{aligned} \Delta \overline{C}_{nm} &= (C_{nm})_{\text{estimate}} - (C_{nm})_{\text{truth}} \\ \Delta \overline{S}_{nm} &= (S_{nm})_{\text{estimate}} - (S_{nm})_{\text{truth}} \end{aligned} \tag{12}$$

and $r_{\oplus}$ is the radius of the Earth. This formulation quantifies the geoid error for each degree in units of length as the difference between the defined truth geophysical signal and its best estimate. This expression is a valid assumption since we are working in a strict simulation environment where the truth of the geophysical signals is known.

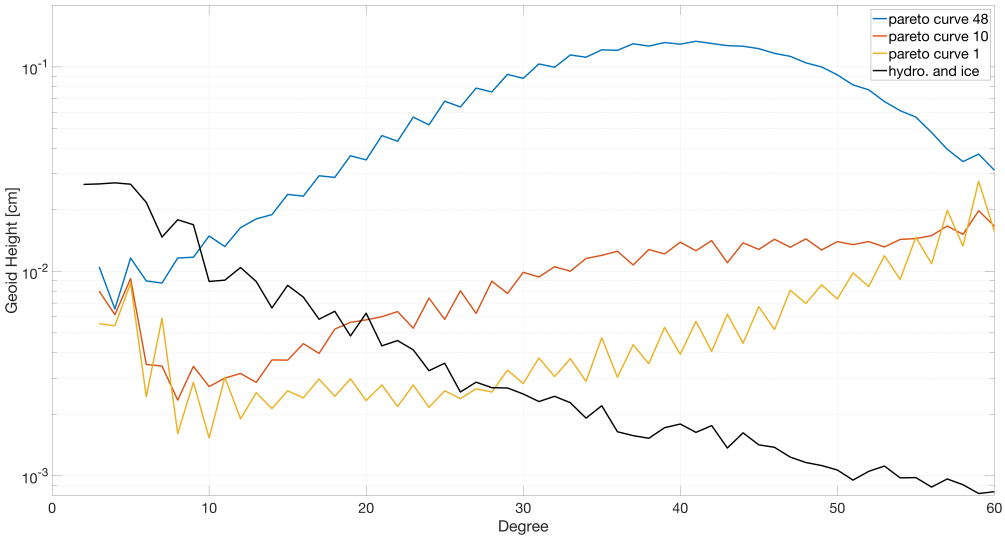

Figure 10. Average degree variances for Pareto curves 1, 10, and 48.

Here, we see that the closer the Pareto curves are to the optimality point, the better low and high degrees can be resolved since their corresponding error, in colored lines, is below the time-varying gravity signal, represented by the black line. The degree variance results for Pareto curve 98 could not be shown since the resulting constellations did not converge onto a usable solution.

Having verified the spatial relation described by our methodology, we will now analyze the final set of GRACE-like constellations. After 20 generations, the GA converged onto a family of ten different constellations, each with six GRACE-like pairs. Figure 11 shows that according to the objective function, these constellations have a slight variation in both spatial as well as temporal coverage.

Figure 10 has shown the spatial relation between the J_{so} and the resulting degree variance from the simulations. To verify the temporal correlation, we perform a temporal analysis of the constellations shown in Figure 11 for a simulation period of one day. For this, we compare the constellations that perform better according to the objective function J_{to} to the ones that do not. From Figure 12, we can see a one-to-one correlation between the quality of the resolved geophysical field in the degree variance curves and the corresponding temporal objective function value.

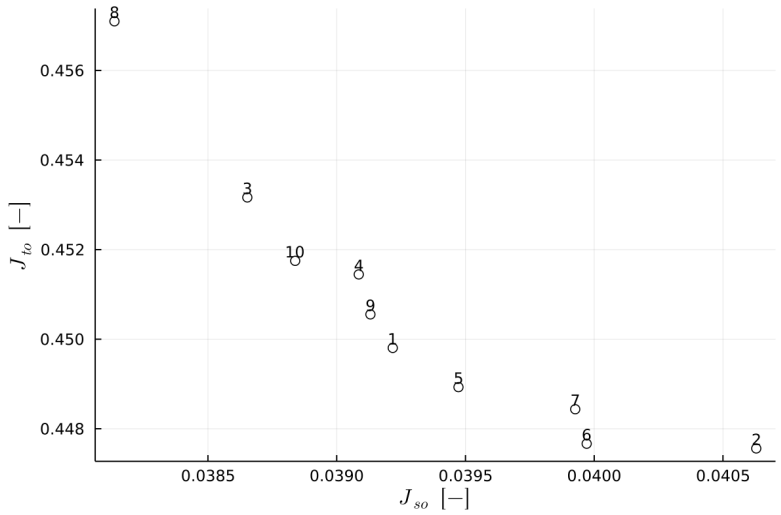

Figure 11. Family of ten six-pair constellations defined by the Pareto front after twenty generations. The values for the objective functions J_{so} and J_{so} are unitless.

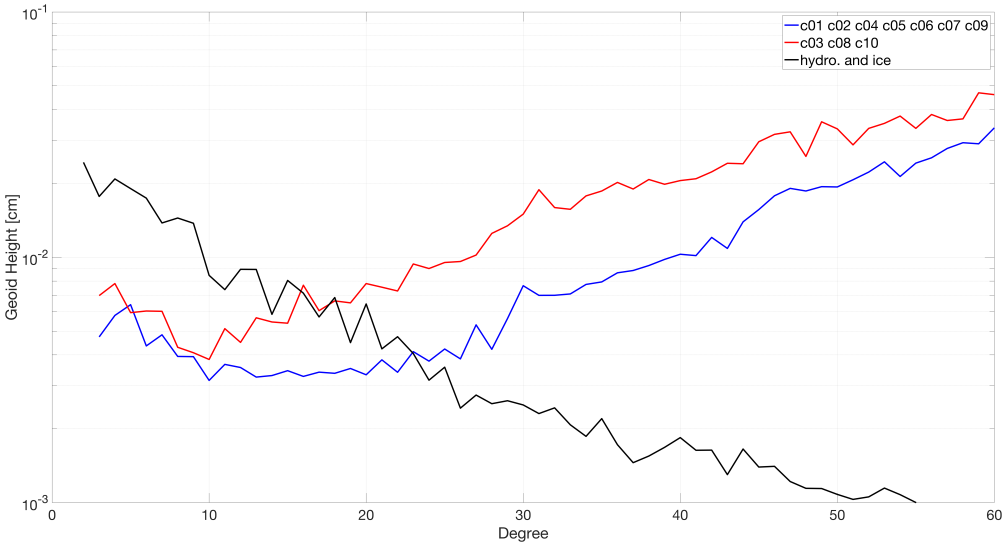

Figure 12. 1-day average degree variances for constellations c01–c10.

Additionally, we analyze the daily variation during the month. For this, we show the daily changes of constellation c06 in Figure 13. Here, we see that the daily degree variance stays within a small variation over one month. This concludes the verification of the transfer function between the designed methodology in Section 2 with the orbital configuration in Section 3 to the simulation setup of Section 4.

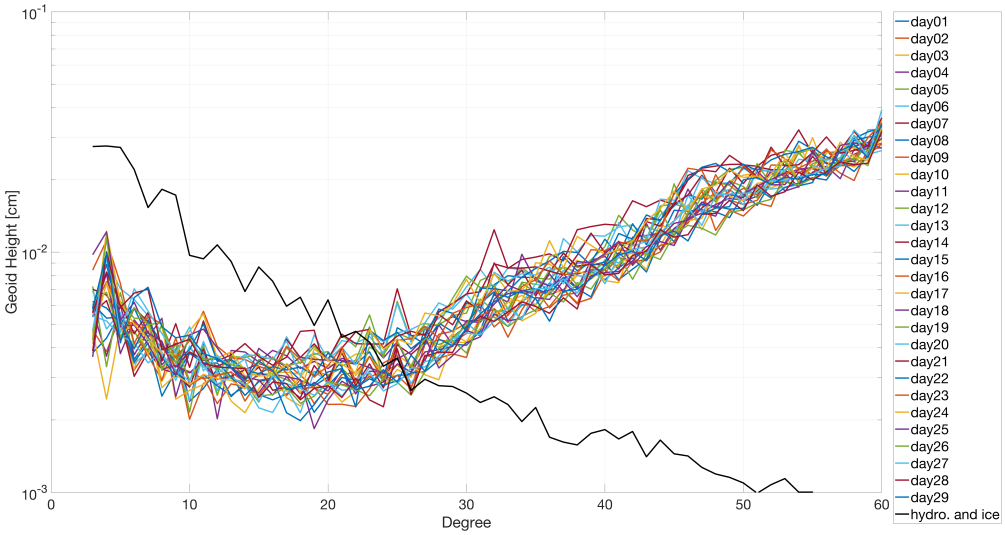

Figure 13. 1-day degree variances for constellation c06 for the month of January 2003.

The 29-day average degree variance curves in Figure 14 show that the spatial resolutions of the selected family of ten constellations from Figure 11 perform equally well over a period of 29 days since there is no significant discrimination in the architectures. Using the temporal objective function to select preferred constellations is most beneficial for shorter time periods (i.e., daily).

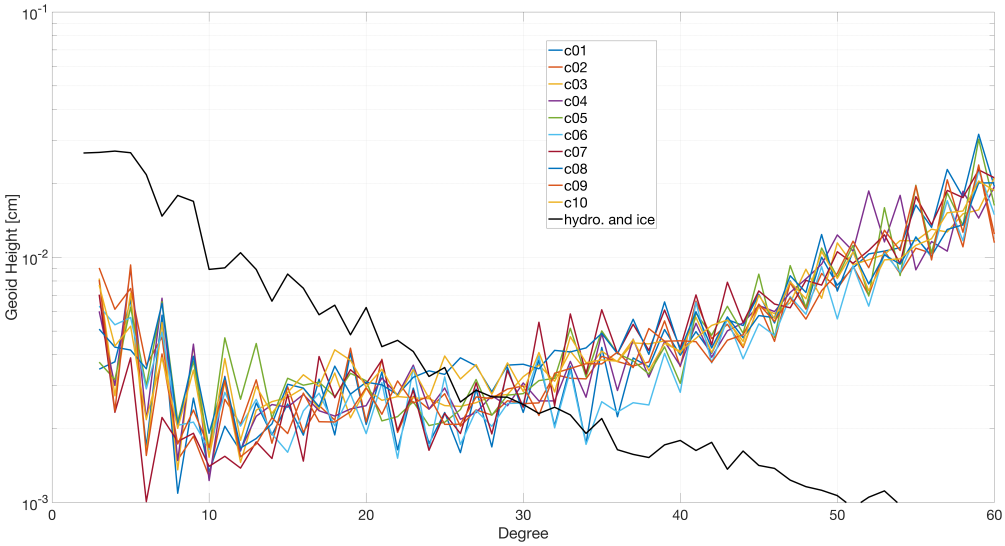

Figure 14. 29-day average degree variances for constellations c01 to c10.

The sawtooth pattern, especially at low degrees, could result from how the data are combined. Currently, each pair is given equal weight in the simulations. We hypothesize that performing spectral weighting when combining the satellite pairs may alleviate this issue. Satellites with very low inclinations have poor observability in specific spectral bands. It may be helpful to down-weight these observations in these bands. Alternatively, mascons or local basis functions could suppress this pattern. This is subject to future study. The Keplerian orbital elements of the constellations shown in Figures 11–14 are shown in Table 4. Here, the inclination i_n, right ascension of the ascending node Ω_n, and mean anomaly M_n are given for each of the six pairs that make up the family of ten final constellations.

Table 4. GA generated six-pair GRACE-like constellations after twenty generations.

id (-)	i_1 (°)	Ω_1 (°)	M_1 (°)	i_2 (°)	Ω_2 (°)	M_2 (°)	i_3 (°)	Ω_3 (°)	M_3 (°)
c01	87.13	78.55	236.16	99.52	168.61	269.94	116.55	33.52	134.84
c02	23.97	258.68	224.9	139.26	146.1	157.35	102.35	157.35	67.29
c03	81.39	179.87	67.29	66.29	112.32	191.13	116.55	292.45	348.74
c04	58.42	134.84	202.39	89.0	44.77	247.42	91.0	360.0	33.52
c05	144.55	112.32	326.23	133.58	247.42	33.52	96.68	112.32	292.45
c06	92.87	269.94	112.32	102.35	360.0	44.77	116.55	337.48	247.42
c07	98.61	236.16	157.35	108.03	44.77	33.52	86.16	360.0	314.97
c08	64.16	292.45	326.23	89.0	337.48	67.29	83.32	146.1	56.03
c09	87.13	269.94	224.9	54.94	157.35	202.39	77.65	179.87	56.03
c10	35.45	247.42	269.94	110.87	281.19	101.06	89.0	134.84	112.32
id (-)	i_4 (°)	Ω_4 (°)	M_4 (°)	i_5 (°)	Ω_5 (°)	M_5 (°)	i_6 (°)	Ω_6 (°)	M_6 (°)
c01	32.23	202.39	168.61	52.1	67.29	112.32	91.0	292.45	11.0
c02	125.06	67.29	326.23	93.84	224.9	360.0	108.03	191.13	78.55
c03	86.16	258.68	78.55	89.0	22.26	236.16	125.06	236.16	360.0
c04	66.29	33.52	281.19	133.58	213.65	168.61	71.97	303.71	202.39
c05	63.45	269.94	112.32	89.0	326.23	247.42	71.97	303.71	67.29
c06	96.68	236.16	112.32	136.42	157.35	247.42	147.77	236.16	269.94
c07	66.29	191.13	348.74	142.1	56.03	157.35	133.58	281.19	191.13
c08	71.97	112.32	67.29	83.32	281.19	78.55	99.52	269.94	360.0
c09	153.45	89.81	348.74	108.03	337.48	78.55	89.0	22.26	213.65
c10	116.55	247.42	67.29	83.32	67.29	314.97	86.16	191.13	326.23

As we can see, each constellation has at least one polar or near-polar pair, with the remaining constellation uniformly covering a large variety of latitude areas with additional pairs in high-latitude regions.

For the following results, constellation six from Table 4 has been used. All constellations perform equally well. This constellation has been selected due to its high temporal resolution in J_{to}, as seen in Figure 11. The logarithm of the actual error resulting from the simulations using constellation six is shown in Figure 15. Here, we see a significant error in C20, as is common in GRACE-like missions.

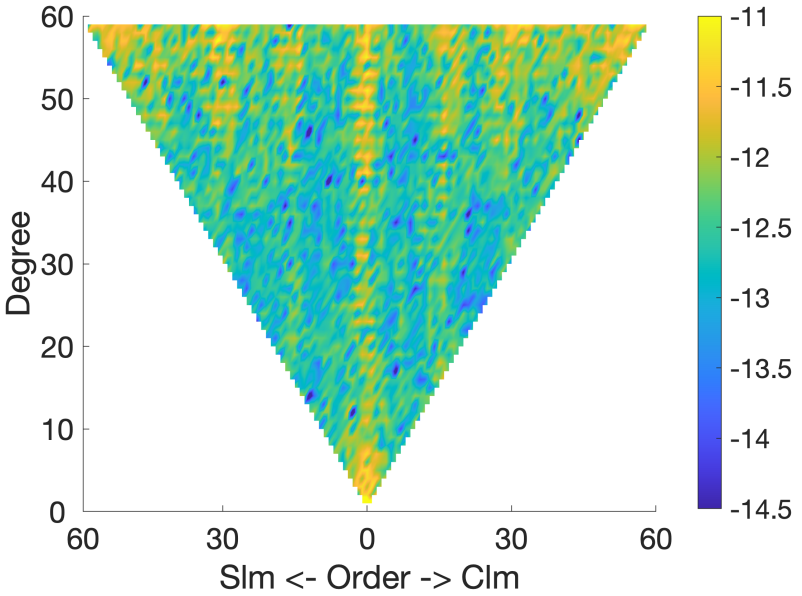

Figure 15. Logarithm of the actual error over a period of 29 days in the recovered signal by constellation six.

In GRACE and GRACE-like designs, it is common to express the disturbing gravitational potential in equivalent water height units. To do this, changes in surface mass density

are defined using the same set of spherical harmonics coefficients previously characterized in Equation (12). The variation in surface mass density is expressed in Equation (13), where $\rho_{\oplus}$ is the mean density of Earth and k stands for the Earth's Love number [61].

$$\Delta\sigma(\phi,\lambda) = \frac{r_{\oplus}\rho_{\oplus}}{3}\sum_{n=0}^{\infty}\sum_{m=0}^{l}\frac{2n+1}{1+k_n}\overline{P}_{nm}(\sin\phi)(\Delta\overline{C}_{nm}\cos m\lambda + \Delta\overline{S}_{nm}\sin m\lambda) \quad (13)$$

To convert the surface mass density in equivalent water height (EWH), it is divided by the density of water ρ_{H_2O}.

Figure 16 shows the spatial representation of the truth hydrology and ice signals along with the recovered signals truncated at degree and order 30 and the corresponding errors. In Figure 16, we see the mean of the daily signal over a period of 29 days of the truth models (top), recovered best estimate (center), and errors in the recovered signal by constellation six (bottom). The C20 pattern dominates over the ocean; so, it is removed for visual comparisons. Due to the size of the constellation and variety of the inclinations present in a six-pair constellation, these solutions have neither been destriped nor smoothed since it was not a necessary step to reduce correlated errors.

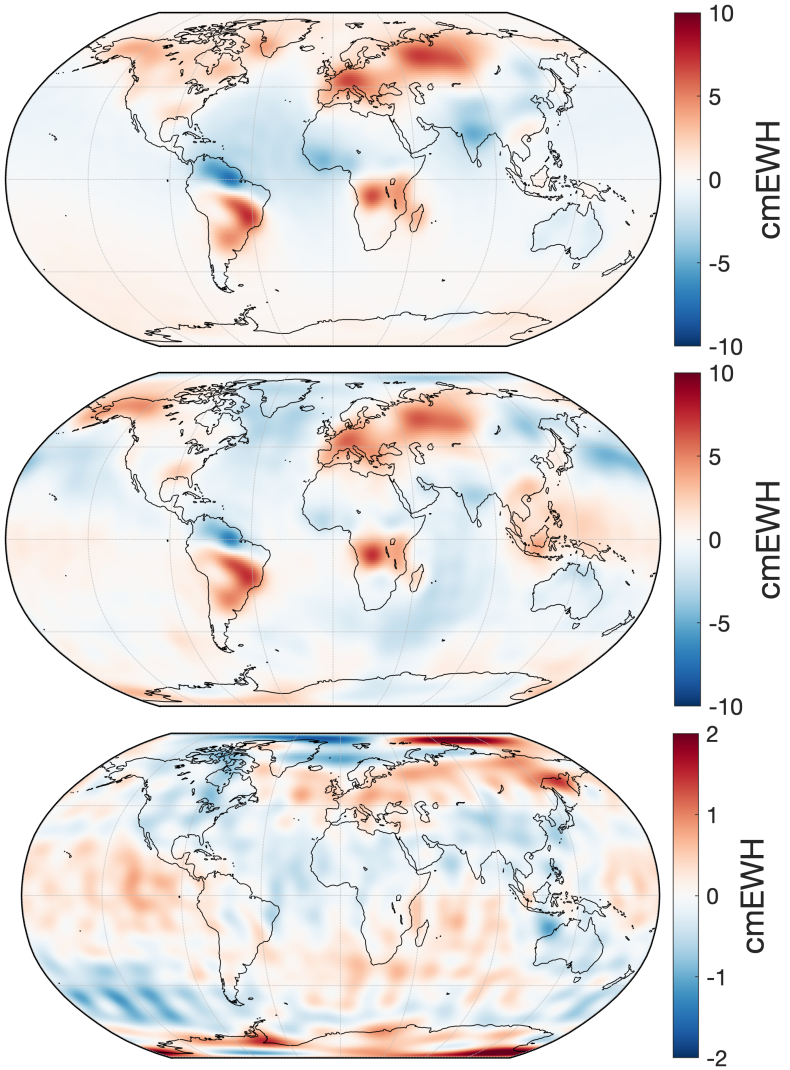

Figure 16. Mean daily signal over a period of 29 days of the truth signal (**top**), the recovered best estimate by constellation six (**center**), and errors in the recovered signal by constellation six (**bottom**). Units are in cm of equivalent water height (EWH) and truncated at degree 30.

6. Conclusions

Due to an increasing trend in the miniaturization of hardware and accelerations in the quality of small form factor satellites, we consider that a future mass change mission could have the shape of an n_{pair} GRACE-like satellite constellation. Such a constellation aims to reduce temporal aliasing by recovering high-frequency temporal variations in the gravitational field. This is achieved through the inherent higher sampling frequency due to the chosen orbit geometry that can be achieved with such an n_{pair} satellite constellation.

The goal of this paper was to develop a tool to optimize the orbits of an n_{pair} GRACE-like satellite constellation to provide increased spatial and temporal resolution in determining hydrology, ice mass variations, and ocean bottom pressure signals globally. The search space for this type of problem is infinite. To efficiently explore the search space, we balance exploration and exploitation with a search algorithm by fixing the altitude at 500 ± 5 km and the number of satellite pairs to six. Although smaller constellations were possible, six satellite pairs were the smallest constellation size to provide a satisfactory recovered gravity field. The constellations have been optimized simultaneously for a monthly and daily time period. We considered only circular orbit in a repeat period of 29 days, which guaranteed us an equal performance on a month-to-month basis. The intersatellite separation amongst satellite pairs has been assumed to be 100 km. Using a fast and elitist multiobjective genetic algorithm as our search algorithm to explore the search space, we developed objective functions that seek to optimize a satellite constellation design regarding uniformity in spatial coverage, ground track directionality, and temporal sampling. These parameters have been calibrated using prior design points and weighted by information on the importance of geophysical signals to equally capture hydrology, ocean, and ice mass variations.

State-of-the-art geodetic parameter estimation and precision orbit determination software provided by NASA's GSFC have been used to verify the geophysical signal recovered by constellations developed by the genetic algorithm. The resulting set of orbital elements describes a family of solutions that, regarding spatial resolution, do not have significant discrimination between the architectures of the different constellations. Due to the temporal objective function, we can discriminate among more suited architectures for shorter (i.e., daily) geophysical recovery. Due to the varying inclinations present in the designed constellations, no postprocessing through destriping nor smoothing was necessary.
The proposed scheme addresses the problem of a future n_{pair} GRACE-like satellite constellation design given by an infinite search space by providing a family with a wide variety of candidate solutions that can be applied for a future mass change study.

Author Contributions: Conceptualization, C.M.A.D., R.S.N., and D.N.W.; methodology, C.M.A.D.; software, C.M.A.D.; validation, C.M.A.D.; formal analysis, C.M.A.D.; investigation, C.M.A.D.; resources, C.M.A.D., R.S.N., and D.N.W.; data curation, C.M.A.D.; writing—original draft preparation, C.M.A.D.; writing—review and editing, C.M.A.D., R.S.N., and D.N.W.; visualization, C.M.A.D.; supervision, R.S.N.; project administration, R.S.N. and D.N.W.; funding acquisition, C.M.A.D., R.S.N., and D.N.W. All authors have read and agreed to the published version of the manuscript.

Funding: This research was funded by the NASA Earth and Space Science Fellowship grant number 18-EARTH18F-0380 and NASA ROSES Earth's Surface and Interior call grant number NNH18ZDA001N-ESI.

Institutional Review Board Statement: Not applicable.

Informed Consent Statement: Not applicable.

Data Availability Statement: The data presented in this study are available on request from the corresponding author.

Acknowledgments: We would like to thank Bryant D. Loomis and Kenneth E. Rachlin from NASA Goddard Space Flight Center for their support in all aspects related to the GEODYN software package. Your help is immensely appreciated.

Conflicts of Interest: The authors declare no conflict of interest.

Abbreviations

The following abbreviations are used in this manuscript:

c	Constellation
ew	East–West
i	Inclination
id	Identification
ns	North–South
ob	Observation
rev	Revisit
ro	Repeat observations
so	Spatial objective function
to	Temporal objective function
ECEF	Earth-centered, Earth-fixed coordinate system
ECMWF	European Centre for Medium-Range Weather Forecasts
EWH	Equivalent Water Height
FES	Finite Element Solution tidal model
GA	Genetic Algorithm
GOT	Goddard Ocean Tide Model
GRACE	Gravity Recovery and Climate Experiment
GRACE-FO	GRACE Follow-On
GSFC	Goddard Space Flight Center
M	Mean Anomaly
MOGA	Multiobjective Genetic Algorithm
MOG2D	2-Dimensional Gravity Waves model
NASA	National Aeronautics and Space Administration
NCEP	National Centers for Environmental Prediction
OMCT	Ocean Model for Circulation and Tides
RAAN	Right Ascension of the Ascending Node
ROSES	Research Opportunities in Space and Earth Science
RP	Repeat period
SC	Spatial cell
TC	Temporal cell

References

1. Tapley, B.D.; Bettadpur, S.; Ries, J.C.; Thompson, P.F.; Watkins, M.M. GRACE measurements of mass variability in the Earth system. *Science* **2004**, *305*, 503–505. [CrossRef]
2. Tapley, B.D.; Bettadpur, S.; Watkins, M.; Reigber, C. The gravity recovery and climate experiment: Mission overview and early results. *Geophys. Res. Lett.* **2004**, *31*. [CrossRef]
3. Tapley, B.D.; Watkins, M.M.; Flechtner, F.; Reigber, C.; Bettadpur, S.; Rodell, M.; Sasgen, I.; Famiglietti, J.S.; Landerer, F.W.; Chambers, D.P.; et al. Contributions of GRACE to understanding climate change. *Nat. Clim. Chang.* **2019**, *9*, 358–369. [CrossRef] [PubMed]
4. Johnson, G.C.; Chambers, D.P. Ocean bottom pressure seasonal cycles and decadal trends from GRACE Release-05: Ocean circulation implications. *J. Geophys. Res. Ocean.* **2013**, *118*, 4228–4240. [CrossRef]
5. Velicogna, I.; Mohajerani, Y.; Landerer, F.; Mouginot, J.; Noel, B.; Rignot, E.; Sutterley, T.; van den Broeke, M.; van Wessem, M.; Wiese, D.N. Continuity of ice sheet mass loss in Greenland and Antarctica from the GRACE and GRACE Follow-On missions. *Geophys. Res. Lett.* **2020**, *47*, e2020GL087291. [CrossRef]
6. Nerem, R.S.; Leuliette, E.; Cazenave, A. Present-day sea-level change: A review. *C. R. Geosci.* **2006**, *338*, 1077–1083. [CrossRef]
7. National Academies of Sciences, Engineering, and Medicine. *Thriving on Our Changing Planet: A Decadal Strategy for Earth Observation from Space*; The National Academies Press: Washington, DC, USA, 2018. [CrossRef]
8. Landerer, F.W.; Flechtner, F.M.; Save, H.; Webb, F.H.; Bandikova, T.; Bertiger, W.I.; Bettadpur, S.V.; Byun, S.H.; Dahle, C.; Dobslaw, H.; et al. Extending the global mass change data record: GRACE Follow-On instrument and science data performance. *Geophys. Res. Lett.* **2020**, *47*, e2020GL088306. [CrossRef]
9. Sneeuw, N.; Flury, J.; Rummel, R. Science requirements on future missions and simulated mission scenarios. In *Future Satellite Gravimetry and Earth Dynamics*; Springer: New York, NY, USA, 2005; pp. 113–142.
10. Pail, R.; Bingham, R.; Braitenberg, C.; Dobslaw, H.; Eicker, A.; Güntner, A.; Horwath, M.; Ivins, E.; Longuevergne, L.; Panet, I.; et al. Science and user needs for observing global mass transport to understand global change and to benefit society. *Surv. Geophys.* **2015**, *36*, 743–772. [CrossRef]

11. Wiese, D.N.; Nerem, R.S.; Lemoine, F.G. Design considerations for a dedicated gravity recovery satellite mission consisting of two pairs of satellites. *J. Geod.* **2012**, *86*, 81–98. [CrossRef]
12. Loomis, B.D.; Nerem, R.S.; Luthcke, S.B. Simulation study of a follow-on gravity mission to GRACE. *J. Geod.* **2012**, *86*, 319–335. [CrossRef]
13. Elsaka, B.; Forootan, E.; Alothman, A. Improving the recovery of monthly regional water storage using one year simulated observations of two pairs of GRACE-type satellite gravimetry constellation. *J. Appl. Geophys.* **2014**, *109*, 195–209. [CrossRef]
14. Hauk, M.; Wiese, D.N. New Methods for Linking Science Objectives to Remote Sensing Observations: A Concept Study Using Single-and Dual-Pair Satellite Gravimetry Architectures. *Earth Space Sci.* **2020**, *7*, e2019EA000922. [CrossRef]
15. Baker, D.N.; Worden, S.P. The large benefits of small-satellite missions. *EOS Trans. Am. Geophys. Union* **2008**, *89*, 301–302. [CrossRef]
16. Bock, D.; Tajmar, M. Highly miniaturized FEEP propulsion system (NanoFEEP) for attitude and orbit control of CubeSats. *Acta Astronaut.* **2018**, *144*, 422–428. [CrossRef]
17. Sandau, R.; Roeser, H.P.; Valenzuela, A. small satellite missions for earth observation. In *New Developments and Trends*; Springer: Berlin/Heidelberg, Germany, 2010.
18. Nolde, M.; Plank, S.; Richter, R.; Klein, D.; Riedlinger, T. The DLR FireBIRD Small Satellite Mission: Evaluation of Infrared Data for Wildfire Assessment. *Remotesensing* **2021**, *13*, 1459. [CrossRef]
19. Caspi, A.; Barthelemy, M.; Bussy-Virat, C.D.; Cohen, I.J.; DeForest, C.E.; Jackson, D.R.; Vourlidas, A.; Nieves-Chinchilla, T. Small Satellite Mission Concepts for Space Weather Research and as Pathfinders for Operations. *Space Weather* **2022**, *20*, e2020SW002554. [CrossRef]
20. Christophe, B.; Foulon, B.; Liorzou, F.; Lebat, V.; Boulanger, D.; Huynh, P.A.; Zahzam, N.; Bidel, Y.; Bresson, A. Status of development of the future accelerometers for next generation gravity missions. In *International Symposium on Advancing Geodesy in a Changing World*; Springer: Cham, Switzerland, 2018; pp. 85–89.
21. Yang, G.; Chen, J.; Numata, K.; Luthcke, S.; Yu, T. *Compact Coherent Laser Ranging (CCLR) (No. GSFC-E-DAA-TN72283)*; NASA: Washington, DC, USA, 2019.
22. Alonso, I.; Alpigiani, C.; Altschul, B.; Araujo, H.; Arduini, G.; Arlt, J.; Badurina, L.; Balaz, A.; Bandarupally, S.; Barone, B.C.; et al. Cold Atoms in Space: Community Workshop Summary and Proposed Road-Map. *arXiv* **2022**, arXiv:2201.07789.
23. Deccia, C.M.A.; Nerem, R.S.; Yunck, T. A SmallSat constellation mission architecture for a GRACE-type mission design. In Proceedings of the 2017 AGU Fall Meeting, New Orleans, LA, USA, 11–15 December 2017.
24. Deccia, C.M.A.; Nerem, R.S.; Wiese, D.N. Designing a GRACE-type satellite constellation for hydrologic science. In Proceedings of the 2018 AGU Fall Meeting, Washington, DC, USA, 10–14 December 2018.
25. Deccia, C.M.A.; Wiese, D.N.; Loomis, B.D.; Nerem, R.S. Design of GRACE-like Small Satellite Constellations for Improved Temporal Gravity Measurements. In Proceedings of the GRACE/GRACE-FO Science Team Meeting 2020, Online, 27–29 October 2020. [CrossRef]
26. Deccia, C.M.A.; Wiese, D.N.; Loomis, B.D.; Nerem, R.S. Design of future Earth observing mass change constellations using small satellites. In Proceedings of the 2020 AGU Fall Meeting, Online, 1–17 Decemver 2020.
27. Deccia, C.M.A.; Nerem, R.S.; Wiese, D.N. Designing an n-pair satellite constellation for recovering daily Earth system mass change using a multi-objective genetic algorithm. In Proceedings of the 2021 GRACE-FO Science Team Meeting, Online, 12–20 October 2021.
28. Deccia, C.M.A.; Wiese, D.N.; Nerem, R.S. Using genetic algorithms to design satellite constellations for recovering daily Earth system mass change. In Proceedings of the 2021 AGU Fall Meeting, Online, 13–17 December 2021.
29. Yunck, T.; Saltman, A.; Bettadpur, S.V.; Nerem, R.S.; Abel, J.; Widner, M.V., IV; Deccia, C.M.A.; Fountain, E.; Franklin, G.; Esterhuizen, S. The Earth Gravitational Observatory Smallsat Constellation for Advanced Gravity Mapping. In Proceedings of the 2017 AGU Fall Meeting, New Orleans, LA, USA, 11–15 December 2017.
30. Yunck, T.; Saltman, A.; Bettadpur, S.V.; Nerem, R.S.; Widner, M.V., IV; Deccia, C.M.A.; Veneziano, A. Design For A Permanent Earth Gravitational Observatory. In Proceedings of the 2018 AGU Fall Meeting, Washington, DC, USA, 10–14 December 2018.
31. Wiese, D.N. Optimizing Two Pairs of GRACE-like Satellites for Recovering Temporal Gravity Variations. Ph.D. Thesis, University of Colorado at Boulder, Boulder, CO, USA, 2011.
32. Sastry, K.; Goldberg, D.; Kendall, G. Genetic algorithms. In *Search Methodologies*; Springer: Boston, MA, USA, 2005; pp. 97–125.
33. Deccia, C.M.A. *Comprehensive Exam Document: Design of a GRACE-Type Small Satellite Constellation to Improve Temporal and Spatial Resolution of Satellite*; University of Colorado at Boulder: Boulder, CO, USA, 2019.
34. Schaefer, R. *Foundations of Global Genetic Optimization*; Springer: Berlin/Heidelberg, Germany, 2007; Volume 74.
35. Deb, K.; Pratap, A.; Agarwal, S.; Meyarivan, T.A.M.T. A fast and elitist multiobjective genetic algorithm: NSGA-II. *IEEE Trans. Evol. Comput.* **2002**, *6*, 182–197. [CrossRef]
36. Savitri, T.; Kim, Y.; Jo, S.; Bang, H. Satellite constellation orbit design optimization with combined genetic algorithm and semianalytical approach. *Int. J. Aerosp. Eng.* **2017**, *2017*, 1235692. [CrossRef]
37. Stern, J.; Wachtel, S.; Colombi, J.; Meyer, D.; Cobb, R. Multiobjective optimization of geosynchronous earth orbit space situational awareness systems via parallel executable architectures. In *Disciplinary Convergence in Systems Engineering Research*; Springer: Cham, Switzerland, 2018; pp. 599–615.

38. Dai, C.Q.; Yu, T.; Chen, Q. Capacity-Oriented Satellite Constellation Design in Disaster Emergency Communication Network. In Proceedings of the 2020 International Conference on Wireless Communications and Signal Processing (WCSP), Nanjing, China, 21–23 October 2020; pp. 666–671.
39. Wijayatunga, M.; Wu, X. An Optimised Satellite Constellation for Bushfire Detection through Edge Computing. *Preprints* **2021**, 2021030071. [CrossRef]
40. Sheng, M.; Zhou, D.; Bai, W.; Liu, J.; Li, J. 6G service coverage with mega satellite constellations. *China Commun.* **2022**, *19*, 64–76. [CrossRef]
41. Bender, T.; McNabb, J.; Birbasov, N.; Bowne, M.; Robertson, B.E.; Sudol, A.; Mavris, D.N.; Lourenco, N. Satellite Formation Design to Enhance Passive Millimeter Wave Imaging Mission Performance. In Proceedings of the AIAA SCITECH 2022 Forum, San Diego, CA, USA, 3–7 January 2022; p. 1881.
42. Watkins, M.M.; Wiese, D N.; Yuan, D.N.; Boening, C.; Landerer, F.W. Improved methods for observing Earth's time variable mass distribution with GRACE using spherical cap mascons. *J. Geophys. Res. Solid Earth* **2015**, *120*, 2648–2671. [CrossRef]
43. Croteau, M.J.; Nerem, R.S.; Merrifield, M.A.; Thompson, P.R.; Loomis, B.D.; Wiese, D.N.; Zlotnicki, V.; Larson, J.; Talpe, M.; Hardy, R.A. Interactive and Approachable Web-Based Tools for Exploring Global Geophysical Data Records. In Proceedings of the 2017 AGU Fall Meeting, New Orleans, LA, USA, 11–15 December 2017.
44. Gini, C. Variabilità e mutabilità. In *Memorie di Metodologica Statistica*; Pizetti, E., Ed.; Libreria Eredi Virgilio Veschi: Rome, Italy, 1912.
45. Swenson, S.; Wahr, J. Post-processing removal of correlated errors in GRACE data. *Geophys. Res. Lett.* **2006**, *33*. [CrossRef]
46. Bender, P.L.; Wiese, D.N.; Nerem, R.S. A possible dual-GRACE mission with 90 degree and 63 degree inclination orbits. In Proceedings of the 3rd International Symposium on Formation Flying, Missions and Technologies. European Space Agency Symposium Proceedings, SP-654 jILA Pub, Noordwijk, The Netherlands, 23–25 April 2018; Volume 8161, pp. 1665–1669.
47. Pavlis, D.E.; Deng, C.; McCarthy, J.J. *GEODYN Operations Manual*; Contractor Report; SGT, Inc.: Greenbelt, MD, USA, 2010.
48. Ullman, R. *SOLVE Program Mathematical Formulation*; Rep. HSTX- G and G-9201; Raytheon ITSS: Greenbelt, MD, USA, 1997
49. Förste, C.; Schmidt, R.; Stubenvoll, R.; Flechtner, F.; Meyer, U.; König, R.; Neumayer, H.; Biancale, R.; Lemoine, J.; Bruinsma, S.; et al. The GFZ/GRGS satellite and combined gravity field models EIGEN-GL04S1 and EIGEN-GL04C. *J. Geod.* **2008**, *82*, 331–346. [CrossRef]
50. Lyard, F.; Lefèvre, F.; Letellier, T.; Francis, O. Modelling the global ocean tides: Modern insights from FES2004. *Ocean. Dyn.* **2006**, *56*, 394–415. [CrossRef]
51. Ray, R.D. A global ocean tide model from TOPEX/POSEIDON altimetry: GOT99.2. In *NASA Technical Memorandum 209478*; Goddard Space Flight Center: Greenbelt, MD, USA, 1999.
52. Klinker, E.; Rabier, F.; Kelly, G.; Mahfouf, J.F. The ECMWF operational implementation of four-dimensional variational assimilation. III: Experimental results and diagnostics with operational configuration. *Q. J. R. Meteorol. Soc.* **2000**, *126*, 1191–1215. [CrossRef]
53. Kalnay, E.; Kanamitsu, M.; Kistler, R.; Collins, W.; Deaven, D.; Gandin, L.; Iredell, M.; Saha, S.; White, G.; Woollen, J.; et al. The NCEP/NCAR 40-year reanalysis project. *Bull. Am. Meteorol. Soc.* **1996**, *77*, 437–470. [CrossRef]
54. Flechtner, F. *AOD1B Product Description Document for Product Releases 01 to 04*; GRACE 327–750. CSR Publ. GR-GFZ-AOD-0001 Rev. 3.1; University of Texas at Austin: Austin, TX, USA, 2007; 43p.
55. Carrère, L.; Lyard, F. Modeling the barotropic response of the global ocean to atmospheric wind and pressure forcing. *Geophys. Res. Lett.* **2003**, *30*, 1275. [CrossRef]
56. Rodell, M.; House, P.; Jambor, U.; Gottschalck, J.; Mitchell, K.; Meng, C.J.; Arsenault, K.; Cosgrove, B.; Radakovich, J.; Bosilovich, M.; et al. The global land data assimilation system. *Bull. Am. Meteorol. Soc.* **2004**, *85*, 381–394. [CrossRef]
57. Van Dam, T.; Visser, P.; Sneeuw, N.; Losch, M.; Gruber, T.; Bamber, J.; Bierkens, M.; King, M.; Smit, M. *Monitoring and Modelling Individual Sources of Mass Distributions and Transport in the Earth System by Means of Satellites*; Technical Report; Final Report, ESA Contract 20403; ESA: Paris, France, 2008.
58. Kang, Z.; Tapley, B.; Bettadpur, S.; Ries, J.; Nagel, P. Precise orbit determination for GRACE using accelerometer data. *Adv. Space Res.* **2006**, *38*, 2131–2136. [CrossRef]
59. Wiese, D.N.; Bienstock, B.; Blackwood, C.; Chrone, J.; Loomis, B.D.; Sauber-Rosenberg, J.M.; Rodell, M.; Baize, R.R.; Bearden, D.; Case, K.; et al. *The Mass Change Designated Observable Study: Overview and Results*; Earth and Space Science Open Archive: Washington, DC, USA, 2022. [CrossRef]
60. Rowlands, D.D.; Ray, R.D.; Chinn, D.S.; Lemoine, F.G. Short-arc analysis of intersatellite tracking data in a gravity mapping mission. *J. Geod.* **2002**, *76*, 307–316. [CrossRef]
61. Farrell, W.E. Deformation of the Earth by surface loads. *Rev. Geophys.* **1972**, *10*, 761–797. [CrossRef]